

Chromatic compensation of light diffraction: Achromatic diffraction-based applications.

Pedro Andrés^a and Vicent Climent^b

^aDepartamento de Óptica, Universidad de Valencia,
46100 Burjassot, Spain.

^bDepartamento de Ciencias Experimentales, Universitat Jaume I,
12080 Castellón, Spain.

ABSTRACT

The scope of this work is the compensation of the chromatic dispersion inherent to free-space light propagation, both in the Fraunhofer and in the Fresnel diffraction region. The cornerstone of our procedure lies in achieving, in a first-order approximation, the incoherent superposition of the monochromatic versions of the selected diffraction pattern in a single plane and with the same scale for all the wavelengths of the incident light. Our novel optical configurations with achromatic properties for the field diffracted by a screen are formed by a proper combination of a small number of conventional diffractive and refractive lenses, providing an achromatic real image of the diffraction pattern of interest. The residual chromatic aberrations in every case are low even when the spectrum of the incident light spreads over the whole visible region. The resulting achromatic hybrid (diffractive-refractive) systems are applied, in a second stage, for implementing several achromatic diffraction-based applications with white light, like wavelength-independent spatial-frequency filtering, achromatic pattern recognition, white-light array generation, and to designing a totally-incoherent optical processor that is able to perform color processing operations under natural illumination (both spatially and temporally incoherent).

Keywords: Incoherent processing, white-light processing, diffractive optical elements, achromatic Fourier transformation, achromatic Fresnel diffraction patterns, achromatic Fourier processing, color pattern recognition, white-light array illuminators.

1. GENERAL INTRODUCTION

Optical systems that use both spatially and temporally coherent illumination have proved to be very useful to designing optical information processing techniques based on Fourier-transforming methods or on Fresnel diffraction properties¹⁻⁴. Nevertheless, the application of these systems has been greatly restricted by some inherent limitations imposed by the use of coherent light, as the available input-output devices, the presence of speckle noise, their sensitivity to environmental factors, and the requirement of grey-level inputs. In spite of this, analog coherent optical processing has been applied with success in many different areas like biometrics⁵, security and encryption⁶, automatic target recognition and object tracking⁷, and optical computing⁸.

The above drawbacks are being overcome by the use of optical processors designed to work under spatially incoherent and/or temporally incoherent illumination⁹⁻¹³. These techniques offer several potential advantages over those performed with coherent light. Their multichannel nature makes them suitable for processing information in a parallel way, and consequently for improving the signal-to-noise ratio. Furthermore, these methods relax the requirements of the light source (permitting the use of different nonlaser sources), reduce the mechanical stability and tolerance requisites of the optical system, and admit more general input objects.

On the one hand, the use of white-light point-source illumination (i.e., temporally incoherent but spatially coherent light) allows to employ broadband spectrum sources, such as gas discharge lamps and light emitting diodes, and specially to deal with color input signals. Nevertheless, propagation of electromagnetic waves in free space is a physical phenomenon that explicitly depends on the wavelength of the light radiation. This well-known fact leads to the chromatic dispersion of the field diffracted by a screen illuminated with a broadband source, both in the Fraunhofer or in the Fresnel diffraction region. For instance, the white-light Fraunhofer diffraction pattern achieved at the back focal plane of a refractive nondispersive objective is an example of pure lateral chromatic distortion, whereas axial and transversal chromatic blurring may occur at the Fresnel diffraction region. This problem restricts severely the spectral bandwidth of the light source used in a conventional diffraction-based optical processor.

Different approaches can be adopted to solve this matter. One way is based in the use of strong dispersive optical elements, which separate spatially the diffraction patterns provided by the different monochromatic components contained in the spectral bandwidth of the incident light¹². These techniques allow one to apply a coherent treatment to each monochromatic channel and, subsequently, to combine the result of the different channels at the output plane. Nevertheless, these methods have to be applied to a discrete number of spectral lines and their practical implementation is rather complex.

Another interesting approach consists in the development of broadband-dispersion compensation techniques, which allow to exploit the whole spectral content of the incoming light¹³. The key of the compensation procedure lies in achieving a wavelength-independent diffraction pattern, i.e., an incoherent superposition of the monochromatic versions of a selected diffraction pattern in a single plane and with the same scale for all the wavelengths of the incident light. Achromatic diffraction systems meet the above requirement in a first-order approximation.

Of course, the achromatization of diffraction patterns also requires specific systems with strongly dispersive optical components. In this work we focus our interest in optical setups that take advantage of the chromatic aberrations associated with diffractive optical elements (DOEs) to achieve the dispersion compensation. Advances in the fabrication of DOEs in the last few years have led them to be a real alternative to refractive optical elements in many applications. Advantages range from the facilities in the design to the aid in the reduction of monochromatic aberrations such as spherical aberration. Thus, they are also playing an important role in the development of novel achromatic optical processors.

On the other hand, some advantages of incoherent optical processing can also be achieved by use of spatially-incoherent monochromatic illumination. Spatially-incoherent processors are linear in irradiance instead of complex amplitude⁹⁻¹¹. In general, an inco-

herent processing system is an imaging system, in which the incoherent spatial impulse response has been tailored for a particular data processing task. Specifically, the irradiance distribution at the output plane of the optical setup is given by a convolution integral between the incoherent point spread function (PSF) and the image irradiance distribution predicted by geometrical optics.

The next step in this research field lies in the design of optical processing systems able to work with white-light spatially-incoherent sources in order to exploit the advantages of natural incoherent illumination. Nevertheless, the use of white light in the preceding incoherent systems introduces an obstacle, again the dependence of the scale of the incoherent PSF –the modulus squared of the Fourier transform of the aperture amplitude transmittance– on the wavelength of the incoming radiation. Thus, recent research on optical processing under both spatially incoherent and temporally incoherent illumination combines incoherent imaging methods with achromatic Fourier transforming ideas.

In this work, we show a series of optical setups designed for chromatic-dispersion compensation of light diffraction in the Fraunhofer region and in the Fresnel region as well. These optical devices are constituted by a proper combination of a small number of conventional refractive objectives and diffractive lenses. The residual chromatic aberrations in every case are low even with white light. In particular, we describe a new quasi-wavelength-independent Fourier transformer with low lateral residual chromatic aberration. The unique properties shown by the above achromatic Fourier and Fresnel processors are applied, in a second stage, to develop achromatic diffraction-based applications with color inputs under white-light point-source illumination, like wavelength-independent spatial-frequency filtering, parallel color pattern recognition, and white-light array generation. On the other hand, these concepts are also the key to implement a totally-incoherent optical processor, able to perform color processing operations under both spatially and temporally incoherent illumination.

The paper is structured in the following parts. First, in section 2, we briefly analyze our different approaches to develop achromatic Fourier transformers and, in particular, we discuss in detail the achromatic Fourier transform properties of a diffractive lens doublet. We emphasize also the behaviour of a wavelength-compensated Fourier transformer completely free of axial residual chromatic aberration. Next, several applications of these optical configurations are described. In particular, we show how to design an achromatic Fourier processor based in one of the previous architectures. Section 3 deals with the design and development of a totally-incoherent achromatic optical processor and its application to color pattern recognition. In section 4, we pay attention to the achromatization of diffraction in the Fresnel region. After reviewing some proposals to obtain achromatic Fresnel diffraction patterns, we describe a very simple diffractive achromatic Fresnel transformer and several applications in the field of free-space optical interconnects with white light. Finally, in section 5 we present the conclusions.

2. ACHROMATIC FOURIER TRANSFORMERS

2.1. Introduction

Several methods to achieve an achromatic Fourier transformation under broadband illumination have been reported in the bibliography. All-glass achromatic Fourier-transform lenses^{14,15} and combinations of holographic and strongly-dispersive refractive

elements in cascade^{16,17} have been employed to reach the above goal. On the other hand, achromatic Fourier transformers combining diffractive lenses and nondispersive refractive objectives are more easily implemented as they only employ commercially available components¹⁸⁻²¹. Here, the chromatic compensation is performed taking advantage of the severe chromatic aberrations associated with diffractive lenses. In particular, a few years ago, we demonstrated the achromatic Fourier-transforming ability of an hybrid (diffractive-refractive) lens triplet²², and more recently of an air-separated diffractive lens doublet^{23,24}. Furthermore, in contrast with the previous proposals, in the last configuration the scale factor of the achromatic Fraunhofer pattern can be tuned to a prescribed value by moving the input along the optical axis of the system.

In all the above cases and as a result of the achromatic correction, a low lateral chromatic aberration remains, whereas an extra residual chromatic error along the optical axis has been added. Recently, a novel optical design for achieving a quasi-wavelength-independent representation of the irradiance of the optical Fourier transform of any diffracting screen has been demonstrated²⁵. The system is constituted by two diffractive lenses and an intermediate achromatic refractive objective, with the input inserted between the first two optical elements. Now, the Fraunhofer diffraction pattern is achieved at the same axial location for all the spectral components of the broadband source, if we neglect the secondary spectrum of the refractive objective.

Some of the previous optical architectures have made it possible the achromatic recording of some Fraunhofer diffraction patterns like Young fringes and Fourier holograms, and to implement certain achromatic optical processing operations in the Fraunhofer region¹⁸⁻²⁶. In particular, it has been possible to obtain the achromatic white-light display of a dual time (or space)-frequency signal representation, such as the Wigner distribution function (WDF) or the ambiguity function (AF), of one-dimensional real signals²⁷. It has also been reported an achromatic joint transform correlator (JTC) for color pattern recognition. This system compensates the chromatic blurring in the recording of the joint Fourier spectrum of the input under white light by using an achromatic Fourier transformer²⁸. In contrast with other suggested polychromatic JTC²⁹⁻³¹, this architecture allow to exploit the full content of the broadband spectrum emitted by the light source.

On the other hand optical Fourier transformers have also been applied to design array illuminators (AIs)³². An AI is an optical systems which is able to transform a plane wavefront into a 2-D array of bright spots in order to supply an array of micro-optical components with equal amounts of light from a single monochromatic point source or to implement 1-to-N free-space optical interconnects³³. Achromatic Fourier transformers have been applied already to design white-light AIs^{34,35}. In this direction, it has been implemented a very simple all-diffractive white-light AI based on a diffractive lenslet array by using achromatic Fourier transforming methods³⁶.

We would like to point out that the optical configuration in Ref.24 has also allowed one to obtain a positive or a negative group velocity dispersion. Thus, it has been found to be suitable for temporal signal processing applications as well as for communication applications (as pulse compression and dispersion compensation device)³⁷.

It is important to emphasize that the above practical achromatic Fourier transformers provide a Fraunhofer diffraction pattern that is achromatic in irradiance, i.e., there is a quadratic phase factor that remains chromatically noncorrected. This fact prevents that a

second setup in cascade, identical to the first one, transforms back to the spatial domain keeping the partial chromatic correction. In spite of this, some researchers have cascaded two achromatic Fourier transformers in irradiance to develop an achromatic processor, which is subsequently optimized^{18,20,38,39}. The last optical devices are compelled to use highly dispersive optical elements and the residual chromatic aberration at the output plane is high because of the cascading effect.

In a different context, some simple broadband optical imaging configurations constituted by diffractive and refractive optical components have been proposed⁴⁰⁻⁴⁴. Combining both achromatic Fourier transforming concepts and diffractive imaging methods, we have developed an achromatic Fourier processor specially designed for color signal processing⁴⁵. The novel optical processor provides an intermediate achromatic real Fraunhofer plane and a final color image without chromatic distortion. In this way, with a single conventional filter, the same spatial filtering operation can be performed simultaneously for all the spectral components of the broadband illuminating source.

As an application of our achromatic Fourier processor we have implemented a color multiple imaging experiment by spatial filtering with a 1-D grating⁴⁶. Furthermore, we have developed a matched filtering experiment for color-invariant recognition of a reference signal inside a colored scene⁴⁷. The proposed white-light correlator uses a single conventional complex filter matched, simultaneously, to all the wavelengths of the incoming radiation. Thus, a reference pattern can be recognized independently of its spectral content. The position of the color correlation peak at the output plane determines the spatial location of the target and the spectral content provides its chromatic composition.

Next, we first describe in section 2.2, the achromatic Fourier transformation properties of an air-separated diffractive lens doublet. The quasi-wavelength-independent Fourier transformer is presented in section 2.3. Finally, some applications of the previous systems are discussed in section 2.4. In particular, we describe how to obtain the Wigner distribution function of a 1-D signal with white light, an achromatic JTC, a white-light Fourier array generator and an achromatic processor.

2.2. Scale tunable achromatic Fourier transformer

In order to describe an all-diffractive Fourier transformer, first let us reformulate the Fourier transforming properties of a diffractive blazed lens (DL) as follows. Let an input transparency, with wavelength-independent amplitude transmittance $t(x,y)$, be illuminated with a white-light point source S located at a normal oriented distance z , as is shown in Fig.1. The DL is located at a distance d from S. As is well known, a DL has an image focal length, Z , which is proportional to the wave number σ of the incident light, i.e.,

$$Z = Z_0 \frac{\sigma}{\sigma_0} \quad , \quad (1)$$

where the constant Z_0 is simply the value of the focal length for the reference wave number σ_0 . Thus, within the paraxial approximation, one can represent its complex amplitude transmittance by the following quadratic phase factor

$$\exp\left[-\frac{i\pi\sigma_0}{Z_0}(x^2 + y^2)\right] \quad . \quad (2)$$

If we assume the usual Fresnel approximations to be valid, it is easy to demonstrate that, aside from irrelevant constant factors, the monochromatic complex amplitude distribution, $U_1(x,y;\sigma,d_1)$, over the transversal plane located at a distance d_1 from DL, is given by

$$\begin{aligned}
 U_1(x, y; \sigma, d_1) = & \exp\left[i\pi \frac{\sigma}{d_1} \left(1 - \frac{\sigma}{Ad_1}\right) (x^2 + y^2)\right] \int_{-\infty}^{\infty} \int_{-\infty}^{\infty} t(x', y') \times \\
 & \times \exp\left[i\pi \frac{\sigma}{(d-z)} \left(\frac{d}{z} - \frac{\sigma}{A(d-z)}\right) (x'^2 + y'^2)\right] \\
 & \times \exp\left[-i2\pi \frac{\sigma^2}{Ad_1(d-z)} (xx' + yy')\right] dx' dy' \quad , \quad (3)
 \end{aligned}$$

where

$$A = \frac{\sigma}{d-z} + \frac{\sigma}{d_1} - \frac{\sigma_0}{Z_0} \quad . \quad (4)$$

Eq. (3) implies that the Fraunhofer diffraction pattern of the input is achieved when the quadratic phase factor inside the integral is unity. This condition is verified for a distance $d_1(\sigma)$ such that

$$d_1(\sigma) = \frac{Z_0 d \sigma}{\sigma_0 d - Z_0 \sigma} \quad . \quad (5)$$

Thus, the axial position of the Fraunhofer pattern is different for each σ . Likewise, we can recognize from Eq.(5) that each monochromatic Fraunhofer plane is located into the conjugate plane through DL of that containing S in terms of the geometrical optics formulation.

By replacing Eq.(5) into the linear phase factor of Eq.(3), we find that the scaling of the above Fourier transformation, evaluated for each σ at the corresponding Fraunhofer plane, is given by

$$\frac{x(\sigma)}{u} = \frac{y(\sigma)}{v} = \frac{z}{\sigma} \frac{d_1(\sigma)}{d} = \frac{Z_0 z}{\sigma_0 d - Z_0 \sigma} \quad , \quad (6)$$

where u and v are spatial frequencies. In this way, the monochromatic versions of the Fraunhofer diffraction pattern of the input transparency provided by DL under broadband spherical-wave illumination appear chromatically dispersed, both axial and laterally. It is important to recognize, from Eqs.(5) and (6), that the ratio $x(\sigma)/u[d+d_1(\sigma)]$ is independ-

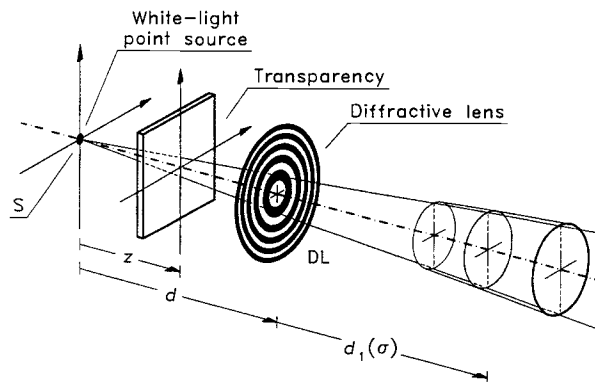


Figure 1. Fraunhofer diffraction pattern of a transparency provided by a diffractive lens under white light.

ent on σ . Thus, the same spatial frequency is located, for each σ , along a straight line directed towards the point source S. In other words, the set of chromatic Fraunhofer diffraction patterns subtend the same angle from the point source S, as is illustrated in Fig.1.

Now, for obtaining the incoherent superposition in a single plane and with the same magnification of the above set of chromatic planar objects, a strong-dispersive optical element is required. To reach the above goal, first, the dispersive imaging element must be inserted at the source plane, in order to achieve the same image size for all the wavelengths simultaneously. This fact implies converging spherical wave illumination, and thus $d < 0$. And second, we choose as imaging element a second DL with a focal length proportional to s as established by Eq.(1).

The optical architecture for achieving the achromatic Fourier transformation is depicted in Fig.2^{23,24}. The complex amplitude distribution at the input plane is then propagated through the system. If we denote by Z'_0 the focal length of DL₂ for the reference wave number σ_0 , the monochromatic field distribution, for the wave number σ , over the transversal plane located at a distance D' from DL₂, $U_2(x,y;\sigma,D')$, can be found as

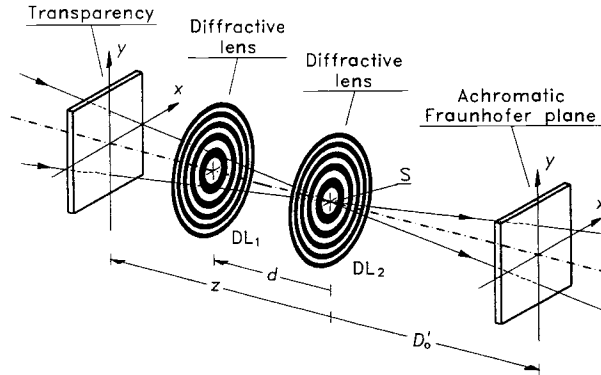


Figure 2. Scale-tunable achromatic Fourier transformer.

$$\begin{aligned}
 U_2(x,y;\sigma,D') = & \exp\left[-i\pi\frac{\sigma}{D'}\left(1+\frac{\sigma}{BD'}\right)(x^2+y^2)\right] \iint_{-\infty}^{\infty} t(x',y') \times \\
 & \times \exp\left[i\pi\frac{\sigma}{(d-z)}\left(\frac{d}{z}-\frac{\sigma}{A'(d-z)}+\frac{\sigma^3}{BA'^2d^2(d-z)}\right)(x'^2+y'^2)\right] \\
 & \times \exp\left[-i2\pi\frac{\sigma^3}{BA'dD'(d-z)}(xx'+yy')\right] dx'dy' .
 \end{aligned} \quad (7)$$

In the above equation the symbols A' and B stand for

$$A' = \frac{\sigma z}{d(d-z)} - \frac{\sigma_0}{Z'_0} , \quad \text{and} \quad B = \frac{\sigma}{d} + \frac{\sigma^2}{A'd^2} + \frac{\sigma_0}{Z'_0} - \frac{\sigma}{D'} , \quad (8)$$

respectively. The irradiance distribution at this plane corresponds to the Fourier transform of the function $t(x,y)$ provided that the quadratic phase factor inside the integral remains equal to unity for all the values of the spatial coordinates x' and y' . By requiring this condition, we conclude that the Fourier transform is achieved at a distance $D'(\sigma)$ given by

$$D'(\sigma) = \left[\frac{1}{d} + \frac{\sigma_0}{Z'_0\sigma} - \frac{Z'_0\sigma}{\sigma_0 d^2} \right]^{-1} . \quad (9)$$

By considering now the linear phase factor in Eq.(7), we find that the scale factor of the Fourier transform achieved at the above plane is

$$\frac{x(\sigma)}{u} = \frac{y(\sigma)}{v} = \frac{zZ_0}{\sigma_0 d^2} D'(\sigma) \quad (10)$$

Both the position and the scale of the Fraunhofer diffraction pattern of the input given by Eqs.(9) and (10) are wavelength dependent and, thus, a chromatic error both axial and transversal appears. Nevertheless, we can achieve an achromatic correction if the derivative of the function $D'(\sigma)$, or equivalently of the scale factor, with respect to the wave number vanishes at a certain reference wave number σ_0 . Note that $D'(\sigma)$ and $x(\sigma)/u$, or $y(\sigma)/v$, are related by a constant factor. In mathematical terms, we require

$$\left. \frac{\partial D'(\sigma)}{\partial \sigma} \right|_{\sigma=\sigma_0} = \left. \frac{\partial x(\sigma)}{\partial \sigma} \right|_{\sigma=\sigma_0} = \left. \frac{\partial y(\sigma)}{\partial \sigma} \right|_{\sigma=\sigma_0} = 0 \quad (11)$$

This requirement leads to the constraint

$$d^2 = -Z_0 Z'_0 \quad (12)$$

which links the focal length of both DL's with the separation between them. By combining this result with Eq.(9) we obtain that the achromatic representation of the Fraunhofer diffraction pattern of the input is located at a distance $D'_0 = D'(\sigma_0)$ from DL₂ such that

$$D'_0 = \frac{d^2}{d - 2Z_0} = \frac{\alpha}{\sqrt{\alpha} - 2} Z_0 \quad (13)$$

where the dimensionless parameter α is

$$\alpha = |Z'_0 / Z_0| \quad (14)$$

From Eq.(13), we infer that to obtain a real achromatic Fourier transformation, i.e. $D'_0 > 0$, DL₁ and DL₂ should be a diverging and a converging lens, respectively, and the parameter α must satisfy the inequality $0 < \alpha < 4$. Another choice of the value of α leads to a virtual achromatic Fraunhofer diffraction pattern and, in this case, an additional refractive objective is required to produce a real image.

As a result of the achromatic correction, a low residual chromatic error still remains. From Eq.(9) we obtain that for each wave number σ the Fraunhofer pattern is just achieved at a distance $D'(\sigma)$, from DL₂, such that

$$D'(\sigma) = \frac{D'_0}{1 + \frac{1}{2 - \sqrt{\alpha}} \frac{(\sigma - \sigma_0)^2}{\sigma \sigma_0}} \quad (15)$$

It is possible to show that the longitudinal and the transversal residual geometrical chromatic aberrations, defined as the fractional differences

$$LCA = 100 \frac{D'_0 - D'(\sigma)}{D'_0} \quad , \quad \text{and} \quad TCA = 100 \frac{x'(\sigma_0) - x'(\sigma)}{x'(\sigma_0)} \quad (16)$$

have an identical analytical expression, here called $CA(\sigma)$, given by

$$CA(\sigma) = \frac{100}{1 + (2 - \sqrt{\alpha}) \frac{\sigma \sigma_0}{(\sigma - \sigma_0)^2}} \quad (17)$$

The chromatic aberration is dependent only on the choice of σ_0 and the value of α . It is convenient to choose σ_0 in such a way that $CA(\sigma_1) = CA(\sigma_2)$ being σ_1 and σ_2 the end wave numbers of the incoming light. Applying this requirement to Eq.(17) we obtain $\sigma_0 = \sqrt{\sigma_1 \sigma_2}$. In this way, the greatest value of the chromatic aberration, CA_M , is

$$CA_M = \frac{100}{1 + \beta(2 - \sqrt{\alpha})} \quad (18)$$

where $\beta = \sqrt{\sigma_1 \sigma_2} / (\sqrt{\sigma_1} - \sqrt{\sigma_2})^2$ takes into account the spectral bandwidth of the incoming light. In Fig.3 we plot the residual chromatic aberration CA vs. σ for two values of α , $\alpha=1$ by continuous line and $\alpha=0.2$ by short dashed line. The lateral chromatic aberration associated with the Fraunhofer diffraction pattern provided by a conventional lens is shown by long dashed line in the same figure. In this plot we assume that $\sigma_1 = \sigma_C = 1.52 \mu\text{m}^{-1}$ and $\sigma_2 = \sigma_F = 2.06 \mu\text{m}^{-1}$, which correspond, respectively, to the labeled C and F Fraunhofer lines for the visible spectrum. Hence, $\sigma_0 = 1.77 \mu\text{m}^{-1}$.

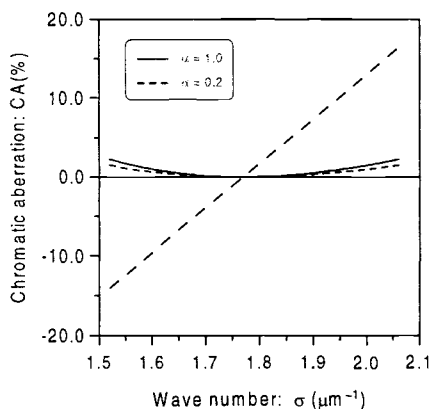


Figure 3. Residual chromatic aberration.

We would like to emphasize that, as is indicated in Eq.(10), the scale factor of the achromatic Fourier transform varies linearly with the distance z between the input transparency and DL_2 . Thus, by simply shifting the input along the optical axis of the system, we can change the magnification of the achromatic Fraunhofer diffraction pattern in a continuous way, but at the same time the degree of achromatization is preserved.

Fig.4 shows a grey-level picture of the irradiance distribution at the achromatic Fraunhofer plane of our proposal when a two-dimensional (2D) square diffraction grating

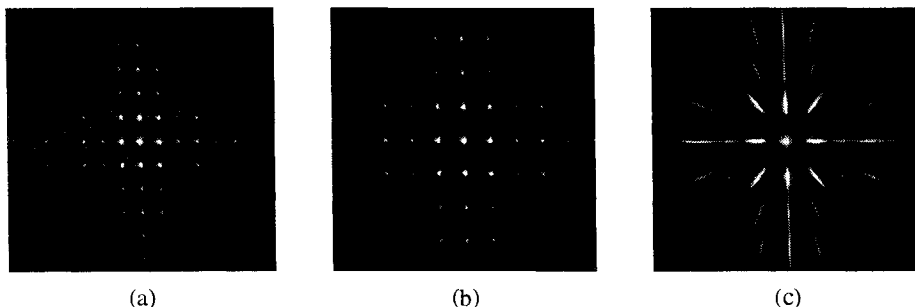


Fig.4. White-light Fraunhofer diffraction patterns of a 2-D grating.

is employed as input transparency. Two different axial locations of the grating were considered in Figs. 4(a) and (b). Note that the location of the diffraction maxima is nearly wavelength independent. For comparison, a grey-level representation of the white-light Fourier transform of the same 2D grating provided by a conventional spherical refractive lens is shown in Fig.4(c). In all the cases we use a Xenon arc lamp as white-light source.

2.3. Quasi-wavelength-independent Fourier transformer

In order to search for a wavelength-compensated Fourier transformer, we consider now the lens arrangement shown in Fig.5²⁵. DL₁ and DL₂ are again two diffractive lenses, with image focal lengths Z₀ and Z'₀ for the reference wave number σ₀, respectively, and the refractive objective L, with focal length f, is inserted between both diffractive elements. Axial distances l and l' denote arbitrary but fixed distances between the elements.

The broadband point source S is imaged through DL₁. Thus, the input diffractive screen, located between DL₁ and L, is illuminated with an axially-dispersed source consisting of a continuum of point sources each radiating at a different σ. The above sources are located at a distance from the input, s(σ), given by

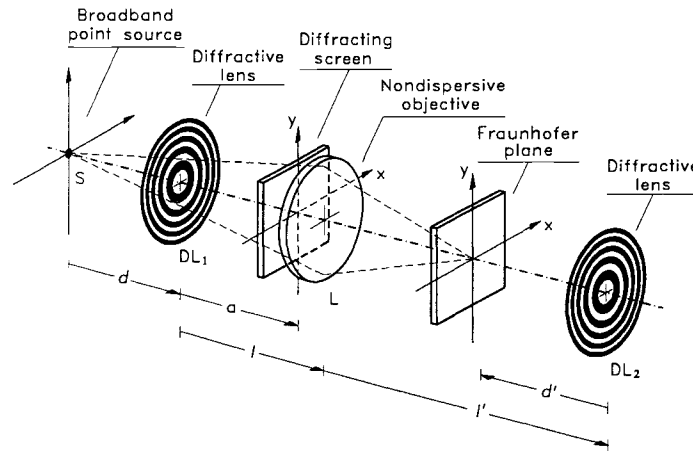


Figure 5. Quasi-wavelength-independent Fourier transformer

$$s(\sigma) = l - [\sigma_0 / (Z_0 \sigma) - 1 / d]^{-1} \quad (19)$$

Now, by propagating the amplitude distribution at the input plane, using the Fresnel diffraction integral, it is possible to show that the monochromatic field amplitude U(x,y;σ), for the wave number σ, over the output plane placed at a distance d' from DL₂ can be written, aside from some irrelevant constant factors, as

$$U(x, y; \sigma) = \exp\left[i\pi\sigma \frac{D}{B}(x^2 + y^2)\right] \times \int \int_{-\infty}^{\infty} t(x', y') \exp\left[i\pi\sigma \frac{A}{B}(x'^2 + y'^2)\right] \exp\left[\frac{-i2\pi\sigma}{B}(xx' + yy')\right] dx' dy' \quad (20)$$

In this equation, t(x,y) denotes the complex amplitude transmittance of the diffracting screen, and parameters A and B are given by

$$A(\sigma) = \left[1 - \frac{d' \sigma_0}{Z'_0 \sigma}\right] \left[1 + \frac{l-a}{s(\sigma)} \left(1 - \frac{l'}{f}\right) + \frac{l'}{s(\sigma)} - \frac{l'}{f}\right] + \frac{d'}{s(\sigma)} \left(1 - \frac{s(\sigma)}{f} - \frac{l-a}{f}\right) \quad (21)$$

$$B(\sigma) = \left[1 - \frac{d' \sigma_0}{Z'_0 \sigma} \right] \left[(l-a) \left(1 - \frac{l'}{f} \right) + l' \right] + d' \left(1 - \frac{l-a}{f} \right) . \quad (22)$$

Next, in order to achieve at the output plane the Fourier transform of the input transmittance $t(x,y)$ for all the wavelength components of the broadband source, we impose the requirement $A(\sigma) \equiv 0$. After some simple mathematical manipulations, Eq.(21) leads to the constraints

$$l' = \frac{f l}{(l-f)} , \quad (23)$$

$$Z'_0 = -\frac{f^2 Z_0}{(f-l)^2} , \text{ and} \quad (24)$$

$$d' = -d \frac{f^2}{(l-f)(d+l-f)} . \quad (25)$$

Eqs.(23) to (25) admit a simple interpretation in terms of geometrical optics. First, DL_1 and DL_2 must have opposite convergence and, aside from this sign, must be conjugated through the lens L. And second, the Fraunhofer plane is located at the conjugate plane through the objective L of that containing the broadband point source S.

Finally, we focus on the wavelength dependence of the scale factor of the Fraunhofer diffraction pattern. An achromatic correction can be achieved if the derivative of the scale factor with respect to σ vanishes at the reference wave number σ_0 , i.e.,

$$\left. \frac{\partial(B/\sigma)}{\partial \sigma} \right|_{\sigma_0} = 0 . \quad (26)$$

Eq.(26) leads to the constraint

$$a = \frac{d Z_0}{2d - Z_0} , \quad (27)$$

which determines, in terms of d and Z_0 , the axial location of the diffractive screen.

As a result of the above chromatic correction, a residual transversal chromatic error $TCA(\sigma)$ still remains. Now there is no axial chromatic error. It is possible to show that $TCA(\sigma)$, expressed as a percentage and referred to the scale factor of the Fraunhofer diffraction pattern for the wave number σ_0 , is

$$TCA(\sigma) = 100 \frac{(\sigma - \sigma_0)^2}{\sigma^2} . \quad (28)$$

From the previous equation, and selecting $\sigma_0 = 2\sigma_1\sigma_2/(\sigma_1 + \sigma_2)$ which assures $TCA(\sigma_1) = TCA(\sigma_2)$, the maximum value of the function $TCA(\sigma)$, denoted by TCA_M , is

$$TCA_M = 100 \left[1 + 2 \frac{1 - \sqrt{1 + (\Delta\sigma/\sigma_0)^2}}{(\Delta\sigma/\sigma_0)^2} \right] , \quad (29)$$

where $\Delta\sigma$ stands for the spectral bandwidth of the illuminating source, $\Delta\sigma = \sigma_2 - \sigma_1$. The dependence of TCA_M on $\Delta\sigma$ is shown by solid curve in Fig. 6. We assume that the end wave numbers of the incoming radiation correspond to the Fraunhofer lines C and F for the visible spectrum. Hence $\sigma_0 = 1.75 \mu\text{m}^{-1}$. The variation on $\Delta\sigma$ of the TCA_M associated with the Fraunhofer pattern provided by a refractive lens is shown by dashed line. The compensation carried out by our setup is a factor of the order of 10 even for white light ($\Delta\sigma = 0.5 \mu\text{m}^{-1}$). It should be emphasized that our design is completely free from longitudinal chromatic aberration.

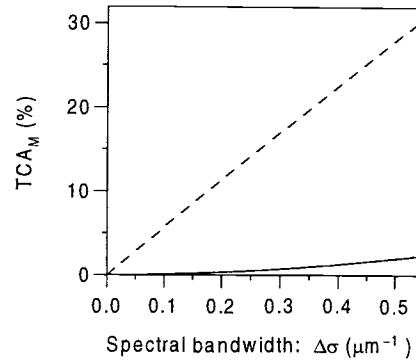


Figure 6. Maximum residual transversal chromatic aberration

To verify the behavior of our quasi-wavelength-independent optical Fourier transformer, we built the optical setup in Fig.5 by following the prescriptions of Eqs.(23) to (25), with $l=2f$, and (27). The object is a conventional computer-generated Fourier hologram. Fig.7(a) shows a gray-level picture of the irradiance distribution at the Fraunhofer plane of our hybrid lens triplet. Reconstruction of the Fourier hologram with white light was successfully achieved. For comparison, a gray-level representation of the white-light Fourier transform of the same Fourier hologram provided by a refractive lens is shown in Fig.7(b). Note the severe chromatic blurring that distort the hologram reconstruction.

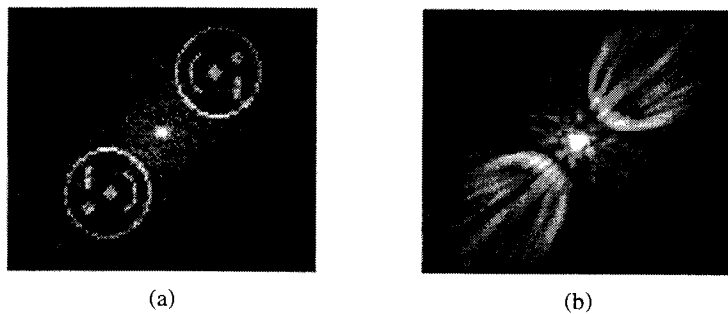


Figure7. Reconstruction of a Fourier hologram under white light.

2.4. Applications

Next, the optical architectures in the previous sections are applied to implement several achromatic Fraunhofer diffraction-based applications working under white light.

2.4.1 Wigner distribution function of a 1-D real signal with white light

The achromatic Fourier transformer in Fig.2 allowed us to obtain the Wigner distribution function (WDF) of a 1-D real signal with white light²⁷. In mathematical terms, the WDF associated to a 1-D real function $f(x)$, $W_f(x,y)$, is

$$W_f(x,y) = \int_{-\infty}^{+\infty} t(x,y') \exp[-i2\pi yy'] dy' \quad , \quad (30)$$

where the function $t(x,y)$ is defined as $t(x,y)=f(x+y/2)f(x-y/2)$. Its achievement by optical procedures involves the simultaneous implementation, on the same output of a 1-D Fourier transform in one direction and a 1-D imaging operation in the orthogonal direction.

The optical setup to perform this operation with white light is shown in Fig.8. L_C is a cylindrical objective and LDL_1 and LDL_2 are two linear diffractive lenses whose active axis are parallel to each other and orthogonal to that of the refractive element. The amplitude transmittance of the input is a scaled version of function $t(x,y)$, built by superimposing two identical transparencies whose amplitude transmittances correspond to the 2-D version of function $f(x)$, each one rotated by an angle θ and $-\theta$, respectively, with respect to the y axis.

The diffractive optical components give rise to an achromatic 1-D Fourier transformation along the y axis, over the output plane, provided that Eq.(12) is fulfilled. Now, d is the separation between both linear diffractive elements, and Z_o and Z'_o are the focal distance of LDL_1 and LDL_2 , respectively, for the reference wave number σ_o . In this way, the achromatic output plane is located at a distance D'_o from LDL_2 given by Eq.(13). By combining Eqs(10) and (13) it is possible to show that the scale factor κ of the Fourier transformation is, in a first-order approximation,

$$\kappa = \frac{y}{v} = \frac{z}{\sigma_o(\sqrt{\alpha}-2)} \quad (31)$$

where v is a spatial frequency and the parameter α is that defined in Eq.(14).

On the other hand, the objective L_C is placed in such a way that the 1-D image of the input plane along the x axis coalesces with the achromatic output plane. Thus, aside from irrelevant constant multiplicative factors, the irradiance distribution at the output plane is an scaled version of the WDF of $f(x)$ modulus squared. Mathematically,

$$I(x, y) = \left| W_f \left(\frac{\cos \theta}{M_x} x, \frac{(\sqrt{\alpha}-2)\sigma_o}{2z \sin \theta} y \right) \right|^2 \quad (32)$$

where M_x is the linear magnification between the input and output planes through L_C .

2.4.2. Achromatic joint transform correlator

As another application of our scale-tunable achromatic Fourier transformer, we have reported an achromatic JTC for color pattern recognition²⁸. Both the color test scene and the reference pattern are displayed simultaneously at the input plane. Then, the diffractive

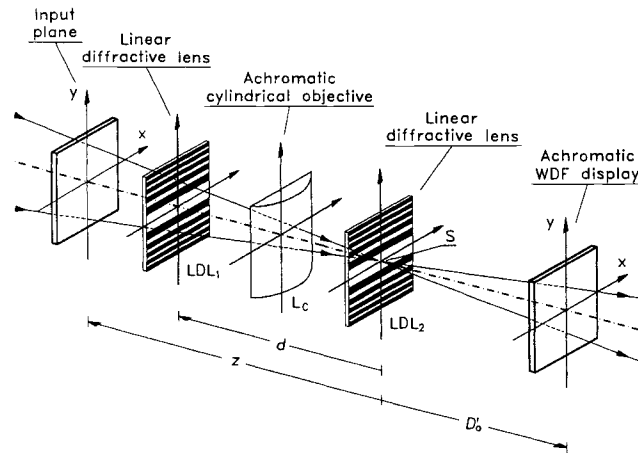


Figure 8. Achromatic Wigner processor.

doublet in Fig.2 allows the register of the joint power spectrum of the input in an achromatic manner with white light. The experimental setup for obtaining the achromatic joint power spectrum is shown in Fig.9. A polychromatic, converging spherical wavefront beam, with end wave numbers σ_1 and σ_2 , impinges on a colour transparency, with amplitude transmittance for the wave number σ

$$t_\sigma(x, y) = f_\sigma(x - x_0, y) + g_\sigma(x + x_0, y) \quad (33)$$

where $2x_0$ is the separation between the input functions $f_\sigma(x,y)$ and $g_\sigma(x,y)$.

The achromatic Fourier transformer is constructed following the prescriptions in section 2.2. In this way, we obtain a real representation of the Fraunhofer diffraction pattern of t_σ with approximately both the same axial location and the same magnification for all σ . The irradiance distribution, $I(x,y)$, at the achromatic Fraunhofer plane is given by

$$I(x, y) = \int_{\sigma_1}^{\sigma_2} \left| \tilde{t}_\sigma \left(\frac{x}{\kappa}, \frac{y}{\kappa} \right) \right|^2 S(\sigma) d\sigma \quad (34)$$

where \tilde{t}_σ denotes the Fourier transform of t_σ , $S(\sigma)$ represents the product of the source spectral distribution and the detector spectral sensitivity, and the scale factor κ is that given by Eq.(31). In particular, if we deal with two objects with the same shape and chromatic distribution, i. e. $g_\sigma(x,y)=f_\sigma(x,y)$ for all σ , Eq.(34) becomes

$$I(x, y) = 2 \{1 + \cos(2\pi 2x_0 x / \kappa)\} \int_{\sigma_1}^{\sigma_2} \left| \tilde{f}_\sigma \left(\frac{x}{\kappa}, \frac{y}{\kappa} \right) \right|^2 S(\sigma) d\sigma \quad (35)$$

The above irradiance distribution consists of a set of modulated interference fringes with approximately the same spatial period for each wavelength.

In a second stage, the achromatic joint power spectrum recorded onto a CCD camera is sent to a liquid crystal TV (LCTV). In the readout process, the LCTV is illuminated with a parallel monochromatic beam, with wave number σ_R . A second Fourier transformation is achieved by using a conventional lens, of focal length f , for obtaining the correlation peak at the back focal plane, as is shown in Fig.9.

It is straightforward to show that for each σ we obtain, at the output plane, the cross-correlation of $f_\sigma(Bx,By)$ with $g_\sigma(Bx,By)$ centered around the points $(\pm 2Bx_0, 0)$,

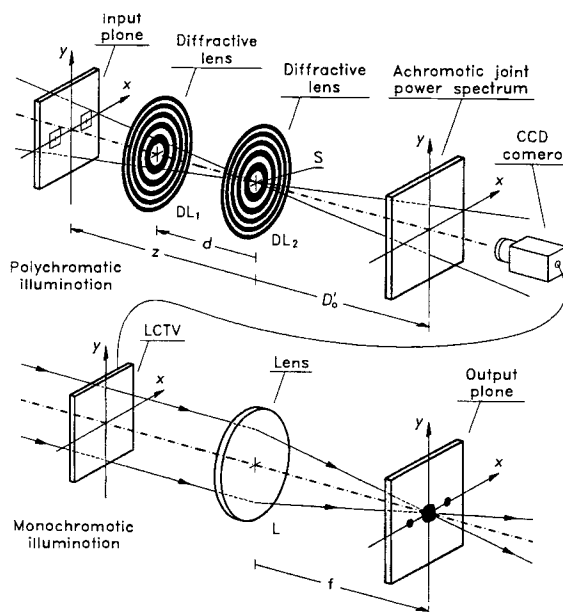


Figure 9. Achromatic joint transform correlator.

where $B = -\kappa\sigma_R/f$. Note that both the origin and the scale factor of the cross-correlation function are σ -independent. Moreover, if $g_\sigma = f_\sigma$ for any σ , i.e., if we deal with a target and a reference object with the same shape for one or a set of chromatic components, the cross-correlation becomes an autocorrelation and an off-axis high-intensity correlation peak is achieved. Thus, a black and white reference pattern will be able to recognize any target with the same shape independently of its chromatic distribution, while a colored reference pattern only will recognize targets with the same shape and spectral content.

2.4.3. White-light diffractive array generator

Diffractive microlens arrays (DLAs) have been employed frequently in the design of AIs. Microlens-based AIs provide high compression and splitting ratio, whereas diffractive optics allows planar structure and 100% fill factor. Nevertheless, they are restricted, in principle, to work under monochromatic illumination. Actually, when a DLA is illuminated by a polychromatic point source S located at a finite distance d , as is shown in Fig.10, the array of light spots results chromatically dispersed, both axially and laterally. By applying the Gaussian lens formula to the imaging process of S through DLA, it can be shown that the array of light dots generated by each σ is located at a distance from DLA given by Eq.(5). Now Z_0 is the focal length of the microlenses for σ_0 . Furthermore, all of the monochromatic arrays subtend the same angle from S . Thus, the array of bright spots generated by DLA are chromatically dispersed just in the same way as the Fraunhofer diffraction pattern in Fig.1.

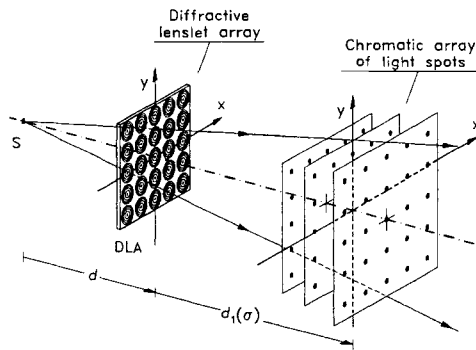


Figure 10. Chromatic dispersion of the array of light spots generated by a DLA under white-light.

In this way, as in the second half of the achromatic Fourier transformer in Fig.2, a single diffractive lens, DL, under converging spherical wave front illumination and inserted at the virtual source plane, can be used for achieving the achromatic superposition of the chromatic array of light spots depicted in Fig. 10. The suggested optical system is shown in Fig. 11³⁶. Following the procedure in section 2.2, the separation d between DLA and DL must fulfill Eq.(12), and the output plane must be located at a distance D'_0 given by Eq.(13). The separation p' between two consecutive achromatic light spots at the output plane is given by

$$p' = p \frac{\sqrt{\alpha}}{(2 - \sqrt{\alpha})}, \quad (36)$$

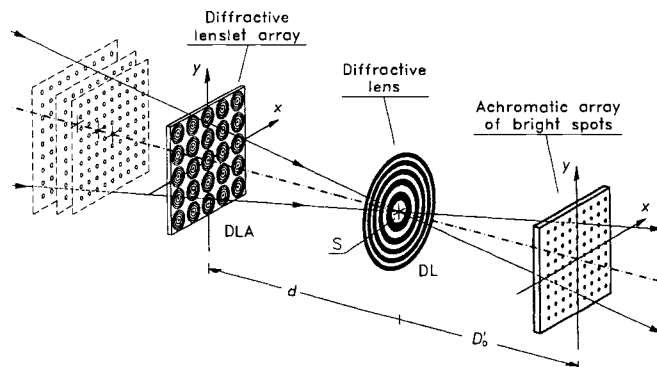


Figure 11. White-light array illuminator based on DLA.

where p denotes the spacing between individual microlenses in DLA, and the parameter α is given by Eq.(14). This simple all-diffractive optical configuration allows to obtain a regularly-spaced set of sharp light spots from a single white-light point-source.

2.4.4. Achromatic Fourier processor

As in previous practical proposals, the achromatic Fourier transformer in Fig.2 provides a Fraunhofer diffraction pattern that is achromatic in intensity. Thus, instead of cascading to similar achromatic Fourier transformers in order to design an achromatic Fourier processor, we conceive the whole optical setup as an achromatic imaging system whose first half performs an achromatic Fourier transformation of the input⁴⁵. In this way, we consider the imaging system shown in Fig.12. It is constituted by two diffractive lenses, DL₂ and DL₃, with focal length Z'_o and Z''_o , respectively, for the reference wave number σ_o , and an achromatic objective L, with focal distance f , located in between. This system can be described in the following simple way in terms of geometrical optics.

Let the input object O, illuminated by a polychromatic light beam, be located at a distance d of DL₂. If we are able, in some way, to compensate the action of the two diffractive lenses, the final image, O', supplied by the optical system will be simply given by the action of the refractive objective L. In this way, we will obtain a wavelength-independent image at the output plane. To this end, first, DL₂ and DL₃ must be located at conjugate planes through L. Thus, the distances l and l' (see Fig.12) must be related by

$$l' = \frac{f}{l-f} l = -M l \quad , \quad (37)$$

where M is the lateral magnification between the conjugate planes. Second, in order that the image of DL₂ through L has the same scale than DL₃, i.e., the same focal distance (aside from a sign change), Z'_o and Z''_o must be linked by the relation

$$Z''_o = -M^2 Z'_o \quad . \quad (38)$$

Thus, the image O' appears just at the conjugate plane of O through the refractive objective L, at a distance d' from DL₃ given by

$$d' = \frac{-f^2}{(l-f)(l+d-f)} d = -M M_o d \quad , \quad (39)$$

where M_o is the lateral magnification between O and O' given by L. Although d' is in principle negative, a real final image can be obtained by adding a second refractive objective at the end of the setup. We can recognize that Ecs.(37) to (39) are the same that Ecs.(23) to (25). This fact corroborates that the achromatic Fraunhofer plane in Fig.5 is located at the conjugate plane through the lens L of that containing the point source S.

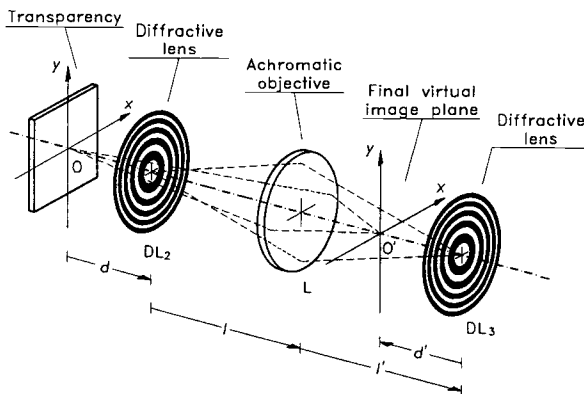


Figure 12. Hybrid imaging system

The appropriate combination of the systems shown in Figs.2 and 11 provides an achromatic Fourier processor as is shown in Fig.13. The first diffractive lenses, DL₁ and DL₂, perform the achromatic Fourier transformation of the input, following the prescriptions of section 2.2. Thus, the

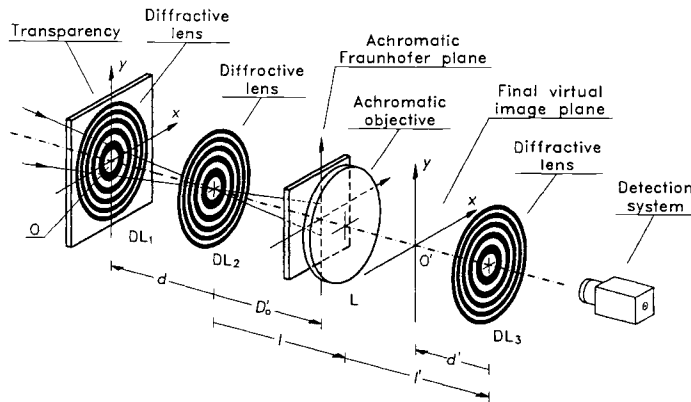


Figure 13. Achromatic Fourier processor.

achromatic condition is fixed by Eq.(12) and the Fraunhofer plane is located at a distance D'_0 from DL₂ given by Eq.(13). The Fourier processor is achieved by adding the achromatic objective L and the third diffractive lens DL₃ in such a way that its position and focal length are determined by Eqs.(37) and (38), respectively. So, the three elements DL₂, L, and DL₃ act as an achromatic imaging system provided that the input be located just against DL₁. The final image is located at a distance d' from DL₃ given by Eq.(39).

This optical Fourier processor provides an intermediate achromatic real Fraunhofer plane and a final color image without chromatic distortion. It is important to note that the formation of the final image can be understood as a double achromatic Fourier transforming process in cascade. In fact, the optical configuration in Fig.13 can be conceived as constituted by a first achromatic Fourier transformer, that in Fig.2, combined with a second quasi-wavelength-independent Fourier transformer, that depicted in Fig.5.

Now, the same spatial filtering operation can be performed simultaneously, with a single conventional filter, for all the spectral components of the broadband source. Thus, this optical configuration is well-adapted for performing achromatic spatial-filtering operations, and consequently is the key for developing different color-invariant pattern recognition techniques. As a first example, we carried out a multiple imaging experiment in which we replicate a color object by inserting a diffraction grating in the intermediate achromatic Fraunhofer plane of the optical system in Fig.13. The input transparency is shown in Fig.14(a). Fig.14(b) shows a gray level picture of the irradiance distribution at the output plane of a conventional refractive 4-f processor with the 1-D grating inserted at

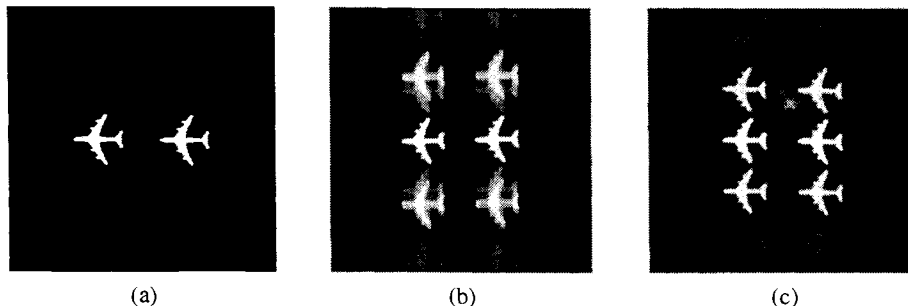


Figure13. Multiple imaging experiment with white light.

the Fraunhofer plane. Fig.14(c) shows the result obtained at the output plane of our achromatic processor when the 1-D grating is used as spatial filter. Note that we obtain multiple copies of the color input with no chromatic artifacts.

3. ALL-INCOHERENT OPTICAL PROCESSOR

3.1. Introduction

As is well known, any spatially-incoherent imaging system can be considered as a diffraction-based spatially incoherent processor. The cornerstone of the procedure consists in tailoring properly the pupil function of the imaging configuration. In this way, it is possible to achieve at the output plane the convolution operation between the input irradiance with the resulting incoherent PSF. Several applications based on this idea have been reported in the literature, in particular for implementing optical correlations under incoherent light⁴⁷⁻⁵¹. These optical processors exploit all the advantages of the use of incoherent light, but also are restricted to work with real and non-negative inputs and outputs.

In incoherent imaging, the spectral bandwidth of the illuminating source is usually of no concern. Nevertheless, the scale of the PSF –the optical Fourier transform of the pupil transmittance– varies linearly with the wavelength. Thus, in optical processing operations, a broad spectrum source produce severe chromatic errors. The above fact restricts the spectral bandwidth that can be employed in an incoherent optical processor.

Recently, we have reported a broadband spatially-incoherent optical processor that performs the convolution of any colour input scene with a reference pattern under natural (both spatial and temporally incoherent) illumination⁵². This novel all-incoherent optical processor, which simply consists of an hybrid lens triplet constituted by two diffractive lenses and a nondispersive refractive objective located in between, is essentially a spatially-incoherent wavelength-independent imaging system that is both linear and shift invariant. In contrast to the conventional case, our optical design exhibits a dispersion-compensated point spread function (PSF).

3.2. All-incoherent optical processor

To discuss the key for implementing the all-incoherent dispersion-compensated optical correlator, let us consider the hybrid (refractive-diffractive) imaging configuration shown in Fig. 12, but now with a spatially and temporally incoherent illuminated transparency as input object. The outline of the optical system is depicted in Fig. 14. DL₁ and DL₂ are again two diffractive lenses, with image focal lengths Z₀ and Z'₀ for σ₀.

Now, in order to include the effects of the aperture transmittance, we evaluate the irradiance distribution for the wave number σ at the image plane, $h(x,y;\sigma)$, due to a single point source, S, located at the origin; i.e., the incoherent PSF. To this end, we recognize that the aperture plane, with amplitude transmittance $p(x,y)$, is illuminated with an axially dispersed source consisting of a continuum of point sources, the images of S through DL₂, each radiating at a different wavelength. It is possible to show that, aside from some irrelevant constant factors, the irradiance distribution at the output plane for each σ is

$$h(x, y; \sigma) = \left| \iint_{-\infty}^{\infty} p(x', y') \exp \left[-\frac{i2\pi\sigma}{B}(xx' + yy') \right] dx' dy' \right|^2, \quad (40)$$

where the coefficient B is

$$B(\sigma) = M_0 \left[\frac{a d \sigma_0}{Z_0 \sigma} - (a + d) \right] \quad (41)$$

In this way, we can write,

$$h(x, y; \sigma) = \left| \tilde{p}(x / \kappa(\sigma), y / \kappa(\sigma)) \right|^2 \quad (42)$$

where \tilde{p} is the 2-D Fourier transform of p and $\kappa(\sigma)$ stands for $B(\sigma)/\sigma$.

The functional dependence of the scale factor $\kappa(\sigma)$ on σ indicates that the scaling of the point source response Fraunhofer pattern is wavelength dependent. So, a transversal chromatic error appears. An achromatic correction can be achieved if we require

$$\left. \frac{\partial \beta}{\partial \sigma} \right|_{\sigma_0} = 0 \quad (43)$$

Eq.(43) leads to the constraint

$$a = \frac{d Z_0}{2d - Z_0} \quad (44)$$

which fixes, in terms of d and Z_0 , the axial location of the pupil plane. Note that this equation is the same than Ec.(27). Thus, the irradiance distribution of the Fraunhofer diffraction pattern generated by the achromatic Fourier transformer in Fig.5 is equivalent to the incoherent PSF of the system in Fig.14, provided that the amplitude transmittance of the input transparency in Fig.5 is the same than that of the aperture function in Fig.14. From Eqs.(41) and (44), the scaling of the dispersion-compensated PSF is

$$\kappa(\sigma) = \frac{M_0 a d (\sigma_0 - 2\sigma)}{Z_0 \sigma^2} \quad (45)$$

As a result of the achromatic correction, a low residual transversal chromatic aberration, TCA , still remains. The value of TCA , expressed as a percentage, is now

$$TCA(\sigma) = 100 \frac{(\sigma - \sigma_0)^2}{\sigma^2} \quad (46)$$

The variation of TCA versus σ is dependent only on the choice of σ_0 . A plot of the function $TCA(\sigma)$ is shown in Fig.15. We select $\sigma_0 = 1.75 \mu\text{m}^{-1}$ and we assume that the ef-

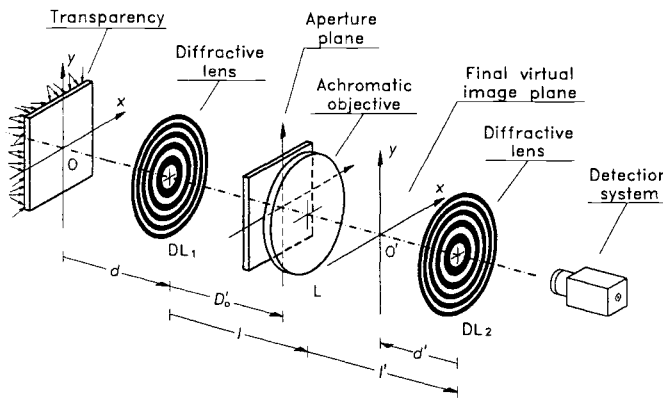


Figure 14. All-incoherent optical processor.

fective end wave numbers of the source are $\sigma_1 = \sigma_c = 1.52 \mu\text{m}^{-1}$ and $\sigma_2 = \sigma_f = 2.06 \mu\text{m}^{-1}$. We obtain that the system in Fig.14 exhibits a dispersion-compensated PSF with a maximum chromatic error less than 2.5% over the entire visible spectrum.

Thus, our optical configuration constitutes a linear and shift invariant system (LSI) with a wavelength-independent PSF in a first order approximation. If we are concerned with an irradiance distribution $I_o(x,y)$ at the input plane, the image plane irradiance distribution, $I_f(x,y)$, is given by

$$I_f(x,y) = I_o(x/M_o, y/M_o) * |\tilde{p}(x/\kappa_o, y/\kappa_o)|^2, \quad (47)$$

where the asterisk symbol denote the convolution operation. Under the above assumption, a wavelength-independent convolution integral between the chromatic-compensated incoherent PSF and the image irradiance distribution predicted by geometrical optics is achieved at the output plane. Hence, our all-incoherent optical processor can perform, with a single filter, the same spatial filtering operation for all the spectral components of the light simultaneously. Now, it is possible to perform a great number of optical processing operations with natural light by choosing properly the pupil transmittance $p(x,y)$.

3.2. Application: Color pattern recognition with natural light.

As a first application of the previous optical architecture, we have carried out a color pattern recognition experiment with natural light⁵². To this end, we use a dispersion-compensated incoherent PSF which is, aside from a sign change, the signal $I_f(x,y)$ we want to detect. If $I_f(x,y)$ is a binary function, the aperture can be implemented as a conventional scaled matched filter, $\tilde{I}_f^*(xM_o/\kappa_o, yM_o/\kappa_o)$, made for coherent filtering.

Fig.16(a) shows a grey-level picture of the color input. Small letters R,G,B and W denote the colors red, green, blue, and white, respectively. Totally incoherent illumination was achieved by illuminating the input with a spatially-incoherent white-light beam arising from the image of the wide arc of a Xenon lamp. The aperture transmittance was constructed as a computer-generated Fourier hologram from which one could reconstruct the

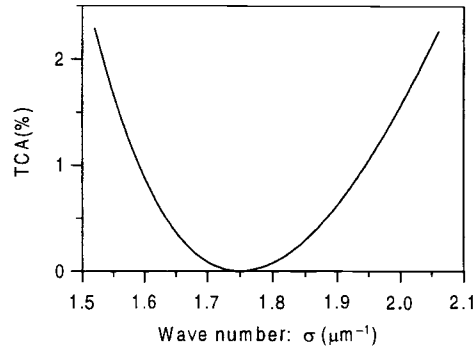


Figure 15. Residual transversal chromatic aberration of the PSF of the system in Fig.14.

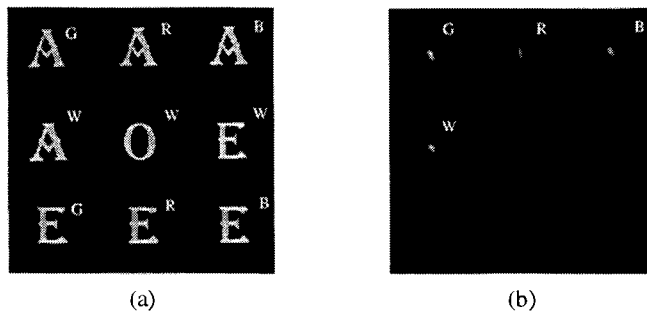


Figure 16. Color pattern recognition experiment performed with all-incoherent illumination.

alphabet letter A. Fig.16(b) shows a grey-level representation of the color irradiance distribution at the output plane of the optical setup in Fig.1. High autocorrelation signals in the chromatic channels where the character A is present are clearly noticeable.

4. ACHROMATIC FRESNEL PROCESSOR

4.1. Introduction

In contrast with Fraunhofer, Fresnel diffraction patterns contain, simultaneously, spatial and frequency information of the input signal and, thus, they seem to be less appropriate to develop information processing techniques. Nevertheless, optical processing in the Fresnel diffraction region is becoming more and more common⁵³. Among other advantages, it allows the design of very simple techniques which, frequently, operate by mere free-space light propagation, and admit space-variant optical data processing.

Concerning achromatic Fresnel diffraction patterns, most of the attention has been paid to obtain achromatic self-images. The Talbot effect, also named self-imaging phenomenon⁵⁴, is a basic property of electromagnetic wavefields under which a set of replicas of certain periodic input structures are achieved without the aid of any lens. Under monochromatic illumination, the above phenomenon has found many practical applications in setting simple and versatile optical information processing techniques⁵⁵.

Several techniques such spectral codification of the source⁵⁶, and Fabry-Perot etalons⁵⁷ have been employed for obtaining wavelength-independent self-images. Nevertheless, the combination of diffractive optical elements and achromatic objectives seems to be a more powerful tool to tackle this subject^{58,59}. The last approach has allowed to record achromatic Fresnel holograms⁶⁰ and a fixed, but arbitrary, achromatic Fresnel diffraction pattern⁶¹. Unfortunately, in all the above cases the components of the optical system have to be specifically designed for each field to be achromatized.

In this direction it has been proposed a single-diffractive lens achromatic Fresnel-transform system working with white-light converging spherical-wave illumination⁶². In contrast to other optical setups previously reported, the axial location of the input permits to vary the Fresnel diffraction pattern that is achromatized. In this way, by simply moving the diffracting screen along the optical axis, we are able to record a continuous range of diffraction patterns with low chromatic aberrations over the entire visible spectrum.

On the other hand, an important method to design AIs is based on Fresnel diffraction³³. AIs that take advantage of the self-imaging phenomenon were firstly introduced by Lohmann⁶³. They are based on the fractional Talbot effect provided by specially designed periodic phase gratings⁶⁴. Recently, several new Talbot AIs have been reported making use of binary phase gratings⁶⁵, multilevel phase gratings⁶⁶, or binary phase gratings in cascade⁶⁷. A general approach for designing Talbot AIs has been presented by Hamam⁶⁸. The use of microlens arrays as phase gratings in a Talbot AI configuration, called by Lohmann modified Talbot AI⁶⁹, seems also very productive⁷⁰. The idea is to combine the high compression and splitting ratio provided by the lenslet array and the flexibility and improved uniformity provided by the fractional Talbot effect. Advantages and limitations of this procedure are discussed by Besold and Lindlein⁷¹.

As an application of our single-diffractive lens achromatic Fresnel transformer we have designed a modified Talbot AI based on the fractional Talbot images - also called

Fresnel images - produced by the set of focal points of a periodic refractive lenslet array under white-light illumination⁷². The achromatic Fresnel-transform setup is able to compensate the chromatic dispersion associated with the Fresnel images of the amplitude distribution at the back focal plane of the lens array. The optical system permits to select the multiplicity of the replica of the array of focal points to be achromatized. In this way, we obtain a very simple AI with a variable density of bright white-light spots at the output plane. In addition, our configuration preserves the high compression ratio provided by the lenslet array and the flexibility and homogeneity provided by the fractional Talbot effect.

In this section, first we point out our approach to achieve achromatic Fresnel diffraction patterns by use of a very simple diffractive lens optical system. Next, we show how to apply this achromatic Fresnel transformer to design a modified Talbot AI based on the fractional Talbot effect exhibited by a periodic refractive lenslet array.

4.2. Achromatic Fresnel diffraction patterns

Let a diffracting aperture, with amplitude transmittance $t(x,y)$, be illuminated with a white-light point source S located at a distance z , as is shown in Fig.17. In this way, an infinite set of diffraction patterns of the input transparency is achieved by free space propagation for each wavelength of the broadband source. The monochromatic amplitude distribution, for each wave number σ , over the transversal plane located at a distance R from the input, $U(x,y;\sigma,R)$, can be described by the following integral equation,

$$U(x,y;\sigma,R) = \exp\left[\frac{i\pi\sigma}{R}(x^2 + y^2)\right] \iint_{-\infty}^{\infty} t(x',y') \exp\left[i\pi\sigma\left(\frac{1}{z} + \frac{1}{R}\right)(x'^2 + y'^2)\right] \times \exp\left[-\frac{i2\pi\sigma}{R}(xx' + yy')\right] dx'dy' \quad (48)$$

where some irrelevant constant factors have been omitted. Eq.(48) indicates that, aside from the spherical wave that precedes the integral, the function $U(x,y;\sigma,R)$ is obtained as the scale Fourier transform of the product of the aperture complex transmittance $t(x,y)$ and the quadratic phase factor $\exp[i\pi\sigma(1/z+1/R)(x^2+y^2)]$.

Thus, a scale version of the above monochromatic irradiance distribution is achieved whenever parameters σ , z , and R are linked through the equation

$$\sigma(1/z + 1/R) = C \quad (49)$$

where C is a real number. In this way, except for a quadratic phase factor, different curvatures and/or wavelengths of the incident wavefront lead to the same irradiance pattern, with different axial location and transversal magnification.

Let us consider now as a reference Fresnel diffraction pattern that located at a distance R_0 from the input transparency under

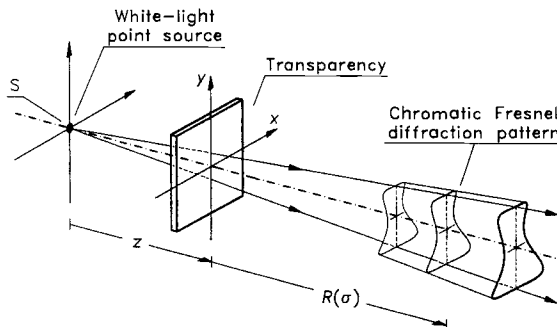


Figure 17. Chromatic dispersion of a Fresnel diffraction pattern under white-light point-source illumination.

monochromatic parallel illumination of wave number σ_0 . For this field, the value of C is

$$C = \sigma_0 / R_0 \quad (50)$$

Combining Eqs.(49) and (50), we obtain that under spherical illumination the reference pattern is located, for each wave number σ , at a distance $R(\sigma)$ from the aperture such that

$$R(\sigma) = \frac{z R_0 \sigma}{z \sigma_0 - R_0 \sigma} \quad (51)$$

Furthermore, the above pattern is obtained with a magnification with respect to the case of parallel illumination with the reference wave number σ_0 , $M(\sigma)$, given by the equation

$$M(\sigma) = \frac{\sigma_0}{\sigma} \frac{R(\sigma)}{R_0} = \frac{z + R(\sigma)}{z} \quad (52)$$

which is derived from the scale factor of the Fourier transformations in Eq.(48) for parallel and spherical illumination. Note, from Eqs.(51) and (52), that under parallel polychromatic illumination the Fresnel patterns are dispersed in such a way that $R(\sigma) = R_0 \sigma / \sigma_0$, and $M(\sigma) = 1$.

Now, as the ratio $M(\sigma)/[z+R(\sigma)]$ is independent on σ , it is clear that the different monochromatic versions of the Fresnel diffraction pattern subtend the same angle from S. Moreover, comparing Eqs.(5) and (51), it is straightforward to recognize that the equations for $d_1(\sigma)$ and $R(\sigma)$ are equivalent if we identify the variables

$$d \rightarrow z, \quad Z_0 \rightarrow R_0 \quad (53)$$

Thus, the above diffraction pattern is chromatically dispersed, both axial and laterally, in the same way as the Fraunhofer diffraction pattern of a transparency provided by a diffractive lens (see Fig.1). This analogy allows to obtain an achromatic representation of the diffraction pattern, with a single DL, by using the same method followed in section 2.2.

The proposed achromatic Fresnel transformer is depicted in Fig.18⁶². The input is illuminated by a broadband point source S, located at a normal distance z , and DL is inserted at the virtual source plane. By performing the substitutions indicated by Eq.(53) into Eqs.(12) and (13) we obtain, first, that the following constraint must be fulfilled

$$z^2 = -Z'_0 R_0 \quad (54)$$

and second, that the achromatic representation of the diffraction pattern is located at a distance D'_0 from DL such that

$$D'_0 = \frac{z^2}{z - 2R_0} = \frac{\alpha}{\sqrt{\alpha} - 2} R_0 \quad (55)$$

where Z'_0 is the focal distance of DL for σ_0 , and the parameter α is defined now as

$$\alpha = |Z'_0 / R_0| \quad (56)$$

Eq.(54) can be understood as follows. Once a diffractive lens with a certain focal length Z'_0 has been chosen, a change in the distance z is equivalent to select a different reference pattern R_0 to be achromatized. Thus, now the axial location of the input permits

achromatize, in a sequential way, different Fresnel diffraction patterns. Eq.(55) provides in each case the axial location of the achromatic diffraction field. From Eq.(55), we note that to obtain a real achromatic image, i.e., $D'_o > 0$, we must select a virtual Fresnel diffraction pattern, with $R_o < 0$, and z must be limited to the domain $|z|/Z_o > 1/2$.

As a result of the achromatic correction, a low residual chromatic aberration still remains.

From the analogy established by Eq.(53), we can recognize that the value of the residual chromatic error for this case is the same than that of the Fraunhofer diffraction patterns in Fig.2. Thus Ecs.(17) and (18) provide the value of the residual chromatic aberration and its maximum value, respectively.

In Fig.19, we report an experimental verification of our procedure. The object, shown in Fig.19(a), is a chirp function, i.e., a linearly increasing spatial frequency object. Under monochromatic illumination, this object is able to focus the incident light into a sharp focal line in certain plane at a Fresnel distance. Nevertheless, under white-light illumination the irradiance distribution at the same plane is affected by a strong chromatic aberration, as is shown in Fig.19(b). In Fig.19(c) we show a grey level representation of the irradiance distribution at the output plane of the system in Fig.18 when the previous object is located as input transparency. It is clearly noticeable the achromatic correction performed by our optical proposal.

4.3. Application: White-light array generation

The achromatic recording of different fractional Talbot images generated by the focal amplitude distribution of a 2-D periodic refractive microlens array (RLA) has allowed us to implement a simple array illuminator with a variable density of white-light spots⁷². Let us consider first a RLA, constituted by microlenses with period p and focal distance f . Its complex amplitude transmittance for the wave number σ can be written as

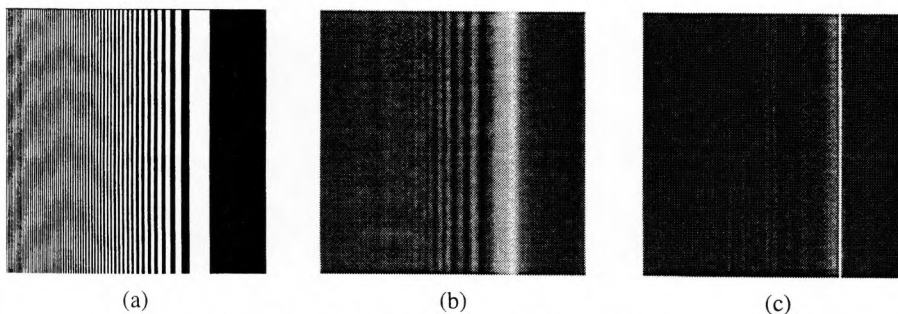


Fig.19. White-light Fresnel diffraction pattern of a chirp function.

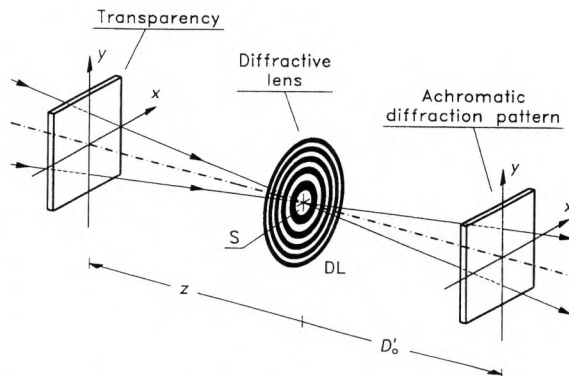


Figure 18. Achromatic Fresnel transformer.

$$t(x, y) = A(x, y) \otimes p(x, y) \exp\left[-\frac{i\pi\sigma}{f}(x^2 + y^2)\right] . \quad (57)$$

In this equation, \otimes denotes the convolution operation, $p(x,y)$ is the pupil function of each lens and $A(x,y)$ is the sampling function which fixes the position of each microlens, i.e.,

$$A(x, y) = \left[\sum_{j=-\infty}^{\infty} \sum_{k=-\infty}^{\infty} \delta(x - jd)\delta(y - kd) \right] , \quad (58)$$

where $\delta(x)$ is the Dirac delta function, and i and j are integer numbers.

It is possible to show that, under parallel monochromatic illumination of wave number σ , the amplitude distribution at a distance R from the focal plane of RLA, $U(x,y;R,\sigma)$, without considering irrelevant constant factors is given by

$$U(x, y; R, \sigma) = \left\{ A(x, y) \otimes \exp\left[\frac{i\pi\sigma}{R}(x^2 + y^2)\right] \right\} \otimes \tilde{p}\left(\frac{x\sigma}{f}, \frac{y\sigma}{f}\right) \exp\left[\frac{i\pi\sigma}{f}(x^2 + y^2)\right] , \quad (59)$$

where \tilde{p} denotes the Fourier transform of p . In particular, at the focal plane, i.e., for $R=0$, the focal intensity distribution looks like a set of sharp intensity peaks, each corresponding to the Fourier transform of the pupil function of a single microlens. On the other hand, the Fresnel diffraction patterns of RLA characterized by Eq.(59) can be understood as the convolution of the Fresnel diffraction patterns of $A(x,y)$ with the Fraunhofer diffraction pattern of each microlens. Thus, as $A(x,y)$ is a periodic function, its Fresnel diffraction patterns will show self-imaging properties and, in particular, they will generate Fresnel images by fractional Talbot effect. These Fresnel images are in turn pinhole arrays.

Under parallel white-light illumination, see Fig.20, the Fresnel images are obtained, for each wave number σ , at a distance R from the back focal plane of RLA given by

$$R = R_0 \sigma / \sigma_0 , \quad (60)$$

where R_0 is the position of the Fresnel image for the reference wave number σ_0 , i.e.,⁷⁰

$$R_0 = (Q + N / N') 2d^2 \sigma_0 . \quad (61)$$

In this equation Q is an integer, and N and N' ($N < N'$) are natural numbers with no common factor. The reduction factor r is equal to N' when N' is odd, and $r = N'/2$ when N' is even. The multiplicity m , i.e., the ratio of the number of bright spots per unit of area of the Fresnel image to that of the original intensity distribution at the focal plane, is $m = r^2$.

From Eq. (60), we recognize that the Fresnel images are dis-

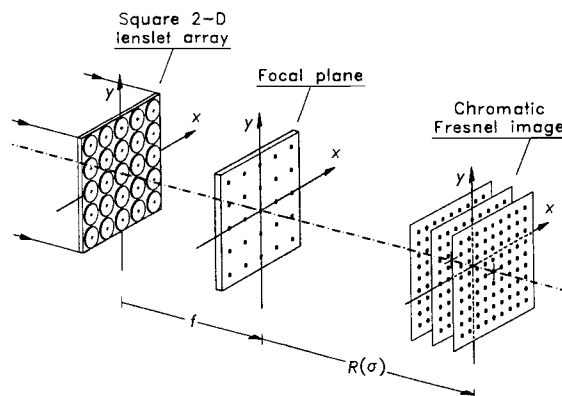


Figure 20. Chromatic Fresnel images of a RLA.

persed in the same way as the Fresnel diffraction patterns of a transparency. Thus, the process of achieving an achromatic copy of a Fresnel image is equivalent to achromatize a Fresnel diffraction pattern with a parameter R_0 given by Ec.(61). The proposed optical setup is shown in Fig.21. The system is built following the prescriptions of section 4.2 and, thus, from Eq.(54), RLA must be placed at a distance h from DL given by

$$h = -f + z = -f - Z'_0 / \sqrt{\alpha} \quad (62)$$

where Z'_0 is the focal length of DL for σ_0 and α is given by Eq.(56). It can be shown that the period p' of the array of bright white-light spots results, in a first-order approximation

$$p' = \frac{\sqrt{\alpha}}{2 - \sqrt{\alpha}} \frac{d}{r} \quad (63)$$

It is important to note that p' can be modified by selecting different Fresnel images which, in general, will have different multiplicity.

In Fig.22 we show an experimental result achieved at the output plane of both a conventional and our achromatic Talbot AI for a Fresnel image generated by the focal amplitude distribution of a RLA. Label (a) is a gray-level picture of the irradiance distribution at the output of the conventional AI for a Fresnel image characterized by $Q=0$,

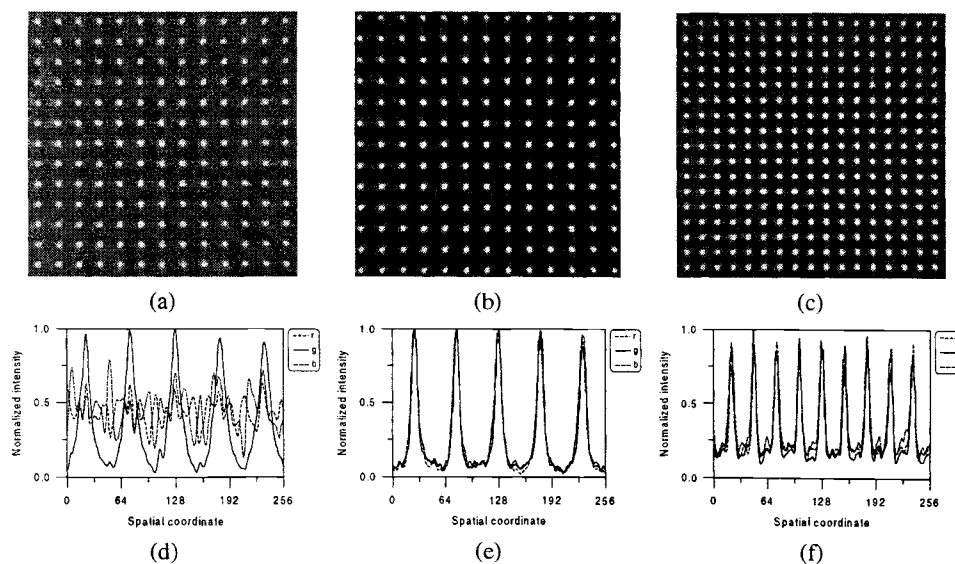


Figure 22. Fresnel images of the focal amplitude distribution of a RLA under white light.

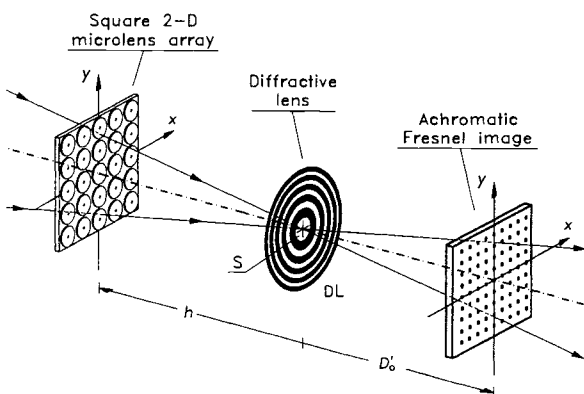


Figure 21. White-light array generator.

$N=1$, and $M=4$, whereas picture labeled (b) show the achromatic result provided by our optical configuration. The achromatic result obtained when we select a second Fresnel image with $Q=0$, $N=1$, and $M=3$ is shown in Fig.23(c). Plots labeled (d), (e), and (f) show the irradiance profile (for each RGB component of the incident light) along a horizontal line obtained by integration of the 2-D irradiance distribution with a vertical slit.

5. CONCLUSIONS

Generally speaking, spatially-coherent but temporally-incoherent optical processors offer several advantages with respect to their coherent counterparts. Among them, we emphasize that they allow to deal with color input signals. Nevertheless, optical incoherent processing techniques must solve the problem of the chromatic dispersion inherent to light diffraction.

To this end, we have proposed different optical configurations, solely formed by a small number of diffractive and refractive lenses, for achieving achromatic diffraction patterns. In all the cases, the residual chromatic aberrations are low even with white-light illumination. In particular, we have designed a scale-tunable achromatic Fourier transformer, a quasi-wavelength-independent Fourier transformer, and a system for achromatizing sequentially the different Fresnel diffraction patterns of any diffracting aperture. Results of laboratory experiments have clearly demonstrated the chromatic compensation carried out by our optical proposals.

Some optical diffractive applications based on these setups have been also described. Specifically, we have presented a white-light Wigner processor, an achromatic joint transform correlator, an optical Fourier processor, a white-light multiple imaging experiment and two different techniques to design white-light array generators.

Moreover, based on the same ideas, we have designed a totally-incoherent optical processor. This system is the key to implement a wide set of novel optical information processing techniques under natural light. As a first example, we have applied this optical configuration to a color pattern recognition experiment.

All the above enumerated techniques have been demonstrated experimentally with conclusive results.

ACKNOWLEDGEMENTS

The authors like to thank J. Lancis, E. Tajahuerce, M. Fernández-Alonso, G. Mínguez-Vega, E. Bonet, and A. Pons for their direct contribution to the work reported herein. An important part of this research has been supported by an agreement between the Universitat Jaume I and the Fundació Caixa Castelló (grant P1B98-14), Spain.

REFERENCES

1. W.T. Cathey, *Optical Information Processing and Holography*, Wiley, New York, 1974.
2. A.W. Lohmann, *Optical Information Processing*, Univ. Erlangen, Erlangen, 1978.
3. H. Stark, *Applications of Optical Fourier Transforms*, Academic, San Diego, 1982.
4. K. Patorski, "The self-imaging phenomenon and its applications," *Prog. Opt.* **27**, 3-108, 1989.

5. P.K.H. Fielding, J.L. Horner, and C.K. Makekai, "Optical fingerprint identification by binary joint transform correlation," *Opt. Eng.* **30**, 1958-1961, 1991.
6. P. Refregier and B. Javidi, "Optical image encryption based on input plane and Fourier plane random encoding," *Opt. Lett.* **20**, 1-3, 1995.
7. A. Pu, R. Denkewalter, and D. Psaltis, "Real-time vehicle navigation using a holographic memory," *Opt. Eng.* **36**, 2737-2746, 1997.
8. J. Jahns and S.H. Lee *Optical Computer Hardware*, Academic, San Diego, 1993.
9. G.L. Rogers, *Noncoherent Optical Processing*, Wiley, New York, 1977.
10. W.T. Rhodes and A.A. Sawchuck, "Incoherent optical processing," in S.H. Lee, ed., *Optical Information Processing: Fundamentals*, ch. 3, Springer Verlag, Berlin, 1981.
11. H. Bartelt, S.K. Case, and R. Hauck, "Incoherent-optical processing," in H. Stark, ed., *Applications of Optical Fourier Transforms*, ch. 12, Academic, Orlando, 1982.
12. F.T.S. Yu, *White-Light Optical Signal Processing*, Wiley, New York, 1985.
13. G.M. Morris and D.A. Zweig, "White-light Fourier transformations," in J.L. Horner, ed., *Optical Signal Processing*, ch. 1.2, Academic, San Diego, 1987.
14. C.G. Wynne, "Extending the bandwidth of stellar speckle interferometry," *Opt. Commun.* **28**, 21-25, 1979.
15. C. Brophy, "Design of an all-glass achromatic Fourier transform lens," *Opt. Commun.* **47**, 364-368, 1983.
16. G.M. Morris, "Diffraction theory for an achromatic Fourier transformation," *Appl. Opt.* **20**, 2017-2025, 1981.
17. G.M. Morris, "An ideal achromatic Fourier processor," *Opt. Commun.* **39**, 143-147, 1981.
18. R.H. Katyl, "Compensating optical systems. Part 3: achromatic Fourier transformation," *Appl. Opt.* **11**, 1255-1260, 1972.
19. R. Ferrière and J.P. Goedgebuer, "A spatially coherent achromatic Fourier transformer," *Opt. Commun.* **42**, 223-225, 1982.
20. R. Ferrière and J.P. Goedgebuer, "Achromatic systems for far-field diffraction with broadband illumination," *Appl. Opt.* **22**, 1540-1545, 1983.
21. S. Leon and E.N. Leith, "Optical processing and holography with polychromatic point source illumination," *Appl. Opt.* **24**, 3638-3642, 1985.
22. P. Andrés, J. Lancis, and W. D. Furlan, "White-light Fourier transformer with low chromatic aberration," *Appl. Opt.* **23**, 4682-4687, 1992.
23. J. Lancis, P. Andrés, W.D. Furlan, and A. Pons, "All-diffractive achromatic Fourier transform setup," *Opt. Lett.* **19**, 402-404, 1994.
24. E. Tajahuerce, V. Climent, J. Lancis, M. Fernández-Alonso, and P. Andrés, "Achromatic Fourier transforming properties of a separated diffractive lens doublet: theory and experiment," *Appl. Opt.* **37**, 6164-6173, 1998.
25. J. Lancis, E. Tajahuerce, P. Andrés, G. Mínguez-Vega, M. Fernández-Alonso, and V. Climent, "Quasi-wavelength-independent broadband optical Fourier transformer," *Opt. Commun.* (submitted).
26. G.D. Collins, "Achromatic Fourier transform holography," *Appl. Opt.* **20**, 3109-3119, 1981.
27. J. Lancis, E.E. Sicre, E. Tajahuerce, and P. Andrés, "White-light implementation of the Wigner distribution function using an achromatic processor," *Appl. Opt.* **34**, 8209-8212, 1995.
28. J. Lancis, E. Tam, A. Pons, and P. Andrés, "Achromatic white-light joint transform correlator: theory and experiment," *Proc. SPIE* **1983**, 419-420, 1993.

29. F.T.S. Yu and Y.S. Cheng, "White-light joint-transform correlator," *Opt. Lett.* **15**, 192-194, 1990.
30. Y.S. Cheng, "Analysis of a white-light joint-transform correlator with application to color-object detection," *Opt. Commun.* **99**, 252-263, 1993.
31. F.T.S. Yu, Z. Yang, and K. Pan, "Polychromatic target identification with a color liquid-crystal-TV-based joint transform correlator," *Appl. Opt.* **33**, 2170-2172, 1994.
32. J.N. Mait, "Fourier Array generators," in *Microoptics*, H. P. Herzig, ed., ch. 11, Taylor & Francis, London, 1997.
33. N. Streibl, "Multiple beamsplitters," in *Optical Computer Hardware*, J. Jahns and S. H. Lee, eds., Academic Press, San Diego, 1993.
34. M. Schwab, N. Lindlein, J. Schwider, Y. Amitai, A.A. Friesem, and S. Reinhorn, "Compensation of the wavelength dependence in diffractive star couplers," *J. Opt. Soc. Am. A* **12**, 1290-1297, 1995.
35. J. Schwider, "Achromatic design of holographic optical interconnects," *Opt. Eng.* **35**, 826-831, 1996.
36. E. Tajahuerce, P. Andrés, J. Lancis, M. Fernández-Alonso, and V. Climent, "White-light array generation with a diffractive lenslet array," *J. Mod. Opt.* **46**, 49-63, 1999.
37. D. Mendlovic, Z. Zalevsky, and P. Andrés, "A novel device for achieving negative or positive dispersion and its applications," *Optik* **110**, 45-50, 1999.
38. G.M. Morris and N. George, "Frequency-plane filtering with an achromatic optical transform," *Opt. Lett.* **5**, 446-448, 1980.
39. R. Ferrière, C. Illueca et J.P. Goedgebuer, "Corrélateur achromatique bidimensionnel," *J. Opt. (Paris)* **17**, 153-159, 1986.
40. J.N. Latta, "Analysis of multiple hologram optical elements with low dispersion and low aberrations," *Appl. Opt.* **11**, 1686-1696, 1972.
41. S.J. Bennett, "Achromatic combinations of hologram optical elements," *Appl. Opt.* **15**, 542-545, 1976.
42. W.C. Sweatt, "Achromatic triplet using holographic optical elements," *Appl. Opt.* **16**, 1390-1391, 1977.
43. I. Weingärtner and K.-J. Rosenbruch, "Chromatic correction of two- and three-element holographic imaging systems," *Optica Acta* **29**, 519-529, 1982.
44. D. Faklis and G.M. Morris, "Broadband imaging with holographic lenses," *Opt. Eng.* **28**, 592-598, 1989.
45. E. Tajahuerce, J. Lancis, V. Climent, and P. Andrés, "Hybrid, (refractive-diffractive) Fourier processor: a novel optical architecture for achromatic processing with broadband point-source illumination," *Opt. Commun.* **151**, 86-92, 1998.
46. P. Andrés and V. Climent, "Chromatic compensation of free-space light propagation combining diffractive and refractive lenses. Achromatic Fresnel and Fourier applications," *OSA Technical Digests Series* **10**, 34-36, 1998.
47. J.D. Armitage and A.W. Lohmann, "Character recognition by incoherent spatial filtering," *Appl. Opt.* **4**, 461-467, 1965.
48. A.W. Lohmann, "Matched filter with self-luminous objects," *Appl. Opt.* **7**, 561-563, 1968.
49. A.W. Lohmann and H.W. Werlich, "Incoherent matched filtering with Fourier holograms," *Appl. Opt.* **10**, 670-672, 1971.
50. J. van der Gracht and J. N. Mait, "Incoherent pattern recognition with phase-only filters," *Opt. Lett.* **17**, 1703-1705, 1992.

51. S. Gorodeisky and A. A. Friesem, "Phase filters for correlation with incoherent light," *Opt. Comm.* **100**, 421, 1993.
52. P. Andrés, V. Climent, J. Lancis, A. Lohmann, G. Mínguez-Vega, and E. Tajahuerce, "All-incoherent dispersion-compensated optical correlator," *Opt. Lett.* (submitted).
53. F. Gori, "Why is the Fresnel transform so little known?", in *Current Trends in Optics*, J.C. Dainty, ed., ch. 10, Academic, London, 1994.
54. J.T. Winthrop and C.R. Worthington, "Theory of Fresnel images. I. Plane periodic objects in monochromatic light," *J. Opt. Soc. Am.* **55**, 373-381, 1965.
55. K. Patorski, "The self-imaging phenomenon and its applications," *Prog. Opt.* **27**, 3-108, 1989.
56. E.E. Sicre, N. Bolognini, and M. Garavaglia, "Partial achromatization of the self-imaging phenomenon," *Appl. Opt.* **24**, 929-930, 1985.
57. G. Indebetouw, "Polychromatic self-imaging," *J. Mod. Opt.* **35**, 243-252, 1988.
58. B. Packross, R. Eschbach, and O. Bryngdahl, "Achromatization of the self-imaging (Talbot) effect," *Opt. Commun.* **50**, 205-209, 1984.
59. J. Lancis, E.E. Sicre, A. Pons, and G. Saavedra, "Achromatic white-light self-imaging phenomenon: an approach using the Wigner distribution function," *J. Mod. Opt.* **42**, 425-434, 1995.
60. R.H. Katyl, "Compensating optical systems. Part 2: generation of holograms with broadband light," *Appl. Opt.* **11**, 1248-1254, 1972.
61. P. Andrés, J. Lancis, E.E. Sicre, and E. Bonet, "Achromatic Fresnel diffraction patterns," *Opt. Commun.* **104**, 39-45, 1993.
62. J. Lancis, E. Tajahuerce, P. Andrés, V. Climent and E. Tepichin, "Single-zone-plate achromatic Fresnel-transform setup: pattern tunability," *Opt. Commun.* **136**, 297-305, 1997.
63. A. W. Lohmann and J. A. Thomas, "Making an array illuminator based on the Talbot effect," *Appl. Opt.* **29**, 4337-4340, 1990.
64. J. R. Leger and G. J. Swanson, "Efficient array illuminator using binary-optics phase plates at fractional-Talbot planes," *Opt. Lett.* **15**, 288-290, 1990.
65. V. Arrizon and J. Ojeda-Castañeda, "Talbot array illuminators with binary phase gratings," *Opt. Lett.* **18**, 1-3, 1993.
66. V. Arrizon and J. Ojeda-Castañeda, "Multilevel phase gratings for array illuminators," *Appl. Opt.* **33**, 5925-45931, 1994.
67. H. Hamam and J. L. de Bougrenet de la Tocnaye, "Multilayer array illuminators with binary phase plates at fractional Talbot distances," *Appl. Opt.* **35**, 1820-1826, 1996.
68. H. Hamam, "Talbot array illuminators: a general approach," *Appl. Opt.* **36**, 2319-2327, 1997.
69. A. W. Lohmann, "Array illuminators and complexity theory," *Opt. Commun.* **89**, 167-172, 1992.
70. E. Bonet, P. Andrés, J. C. Barreiro, and A. Pons, "Self-imaging properties of a periodic microlens array: versatile array illuminator realization," *Opt. Commun.* **106**, 39-44, 1994.
71. B. Besold and N. Lindlein, "Fractional Talbot effect for periodic microlens arrays," *Opt. Eng.* **36**, 1099-1105, 1997.
72. E. Tajahuerce, E. Bonet, P. Andrés, C.J. Zapata-Rodríguez, and V. Climent, "White-light modified Talbot array illuminator with a variable density of light spots," *Appl. Opt.* **37**, 4366-4373, 1998.